

Optimal Distributed Frequency and Voltage Control for Zonal Electricity Markets

Lukas Kölsch, Lena Zellmann, Rishabh Vyas, Martin Pfeifer, and Sören Hohmann

Abstract—Zonal pricing is a well-suited mechanism to incentivize grid-supporting behavior of profit-maximizing producers and consumers operating on a large-scale power system. In zonal electricity markets, local system operators create individual price zones, which provide appropriate price signals depending on local grid conditions such as an excess or shortage of electrical energy in certain regions. In this paper, a continuous-time zonal pricing controller for AC power networks is presented that ensures frequency and voltage stability as well as Pareto efficiency of the resulting closed-loop equilibria. Based on a dynamic network model taking into account line losses and power exchange with adjacent price zones, distributed control laws are derived which require only neighbor-to-neighbor communication. Case studies on the IEEE-57 bus system with different pricing concepts illustrate how zonal prices enable consideration of regional supply and demand conditions as well as increased robustness compared to an isolated grid operation.

Index Terms—real-time pricing, power generation dispatch, frequency control, voltage control, energy cells, AC microgrids.

I. INTRODUCTION

AS a result of the worldwide trend towards more renewable power generation and the displacement of large conventional power plants, there is an increasing number of small-scale generation. A major challenge of this trend is the growing complexity and heterogeneous nature of the future power system consequent from different types of distributed generation units, such as conventional synchronous generators (SGs), renewable energy sources (RESs), and power consuming loads. From an optimization-theoretic perspective, the interaction between these competitive grid participants can be interpreted as a constrained multi-objective optimal control problem, where the objective functions are given by the individual profits and the constraints are imposed by physical laws as well as technical and/ or operational regulations.

Literature Review: The existing literature mainly deals with centralized or sometimes distributed optimization problems, but the majority of work considers only one objective function. For this problem class, the primal-dual gradient method [1] allows to derive continuous-time feedback controllers, which has already been successfully applied in particular aspects of power system control such as frequency regulation [2]–[4], voltage regulation [5] or optimal power flow [6], [7]. A detailed discussion of current research work on optimization-based control of power systems in continuous

time can be found in [8]. By applying the primal-dual gradient method, the Lagrange multipliers of the local power balance constraints are associated with the marginal costs of generation, which turns the gradient ascent of the dual variables into a real-time dynamic pricing controller (cf. [9], [10]).

In the context of multi-objective optimization, the literature is scarce. Two recent papers [11] and [12] develop a Bertrand competition model between price-setting generators resulting in a continuous-time bidding process against a centralized system operator, which is shown to provide economic efficiency. The authors of [13] propose a distributed dynamic pricing mechanism by feedback optimization for a Cournot model of competition between price-setting generators and price-taking (i.e. flexible) loads. However, both approaches rely on the simplifying assumptions of constant voltage magnitudes and zero line losses, i.e. they do not account for the physical system.

Another promising approach to organize a fully decentralized power system is the *web of cells* (WoC) concept [14], [15], where the overall system is divided into interconnected subsystems. Each cell is monitored and controlled by a techno-economic *cell coordinator* (CC), which is responsible for providing frequency and voltage stability within its own cell by applying zonal (i.e. cell-specific) price incentives. Due to their connection via transmission lines, the cells interact with each other, i.e. they explicitly deal with their physical relations. However, to the best of the authors' knowledge, there exists no explicit price-based feedback control strategy for a WoC scenario to date.

Statement of Contributions: In this paper, we derive a distributed, continuous-time zonal pricing controller for lossy AC power networks. For this purpose, we combine a feedback controller for multi-objective optimization with the WoC concept, enabling incentive-based regional price differences as well as power flows across cell boundaries. In line with the WoC concept, our work assumes a mixture of price-taking power plant operators (PPOs), price-setting CCs, and inflexible consumers. The simultaneous execution of distributed controllers results in a dynamic pricing procedure, which ensures both Pareto-efficient allocations as well as frequency and voltage stability. Since the individual resources of a PPO may be located at geographically distant nodes in different cells, this allows the integration of Virtual Power Plant (VPP) operators aggregating a large number of distributed small-scale RESs. The cell-based control architecture allows a global exchange of power, while measurement and control information is only shared locally. In particular, none of the individual profits or costs need to be disclosed by the network participants. The controller design

L. Kölsch, L. Zellmann, R. Vyas, M. Pfeifer, and S. Hohmann are with the Department of Electrical Engineering and Information Technology, Karlsruhe Institute of Technology, Karlsruhe, Germany. (e-mail: lukas.koelsch@kit.edu).

This work was funded by the Deutsche Forschungsgemeinschaft (DFG, German Research Foundation) – project number 360464149.

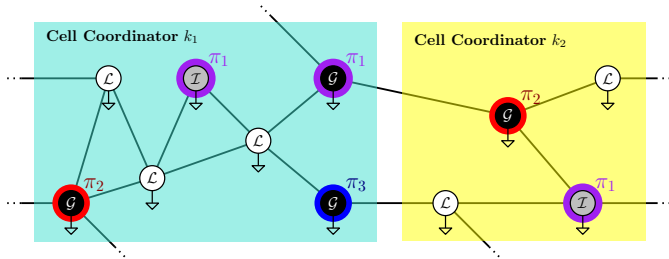


Fig. 1. Schematic WoC network with $\mathcal{P} = \{\pi_1, \pi_2, \pi_3\}$ and $\mathcal{Z} = \{k_1, k_2\}$. Each node of the network is of either \mathcal{G} (black), \mathcal{I} (grey), or \mathcal{L} type (white).

is applicable for power systems with both conventional and renewable network connectors and inflexible loads.

Paper Organization: Section II presents the network model. Section III formulates the optimization problems of the individual network participants and provides a deduction of continuous-time distributed controllers. Section IV extends the controller towards a WoC scenario with mutually related zonal prices and studies the Pareto efficiency of the closed-loop equilibrium. A simulation study using the IEEE 57-bus system is carried out in Section V, while Section VI gives the conclusion and proposes directions for future research.

Notation: Vectors and matrices are written in boldface. All vectors defined in the paper are column vectors $\mathbf{a} = \text{col}\{a_i\} = \text{col}\{a_1, a_2, \dots\}$ with elements a_i , $i = 1, 2, \dots$. All-zeros and all-ones vectors with n entries are denoted by $\mathbf{0}_n$ and $\mathbf{1}_n$, respectively. The $(n \times n)$ -identity matrix is denoted by \mathbf{I}_n . Positive definiteness of a matrix is denoted by $\succ 0$. For $\mathbf{a} \in \mathbb{R}^n$, we write $\mathbf{a} > \mathbf{0}_n$ if each component in \mathbf{a} is greater than zero. Upper and lower bounds are denoted by $\overline{(\cdot)}$ and $\underline{(\cdot)}$, respectively. For a given $\mu \geq 0$, define

$$\langle x \rangle_{\mu}^{+} := \begin{cases} x, & \mu > 0 \vee x \geq 0, \\ 0, & \text{else.} \end{cases} \quad (1)$$

If x and μ are vectors of the same size $i \in \mathbb{N}$, then (1) can be applied component-wise, i.e. $\langle x \rangle_{\mu}^{+} : \text{col}_i\{\langle x_i \rangle_{\mu_i}^{+}\}$.

II. MODELING OF PHYSICAL NETWORK

The underlying physical network is represented by a directed graph $\mathcal{G}_p = (\mathcal{V}, \mathcal{E}_p)$, where the set of nodes $\mathcal{V} = \mathcal{V}_{\mathcal{G}} \cup \mathcal{V}_{\mathcal{I}} \cup \mathcal{V}_{\mathcal{L}}$ is partitioned into generator (\mathcal{G}), inverter (\mathcal{I}), and load nodes (\mathcal{L}). \mathcal{G} nodes are fed by SGs of e.g. gas or hydro turbines. \mathcal{I} nodes are connected to power electronics interfaced RESs such as photovoltaic power stations and \mathcal{L} nodes are connected to inflexible consumers only. \mathcal{G} and \mathcal{I} nodes are equipped with an active power generation input $p_{g,i}$. Inflexible consumers may also exist at \mathcal{G} , \mathcal{I} , and \mathcal{L} nodes, which is expressed by an active power consumption input $p_{\ell,i}$ for all $i \in \mathcal{V}$. Note that $p_{\ell,i}$ may be negative. We assume that subtransient dynamics of the SGs can be neglected. Moreover, it is assumed that the inverter interface at \mathcal{I} nodes is equipped with an internal matching controller [16], [17]. This allows to use the following dynamic network model for our considerations [2], [18]:

$$\dot{\vartheta}_{ij} = \omega_i - \omega_j, \quad i, j \in \mathcal{V}, \quad (2)$$

$$\dot{L}_i = -A_i \omega_i + p_{g,i} - p_{\ell,i} - p_i, \quad i \in \mathcal{V}_{\mathcal{G}} \cup \mathcal{V}_{\mathcal{I}}, \quad (3)$$

$$\tau_{d,i} \dot{U}_i = U_{f,i} - U_i - (X_{d,i} - X'_{d,i}) U_i^{-1} q_i, \quad i \in \mathcal{V}_{\mathcal{G}}, \quad (4)$$

$$0 = -A_i \omega_i - p_{\ell,i} - p_i, \quad i \in \mathcal{V}_{\mathcal{L}}, \quad (5)$$

$$0 = -q_{\ell,i} - q_i, \quad i \in \mathcal{V}_{\mathcal{L}}, \quad (6)$$

where ϑ_{ij} is the voltage angle deviation between nodes i and j , ω_i is the frequency deviation from the nominal frequency, L_i is the angular momentum deviation, A_i is a positive damping coefficient, $\tau_{d,i}$ is the direct-axis transient open-circuit time constant, $U_{f,i}$ and U_i are the excitation voltage and internal voltage magnitudes, $X_{d,i} - X'_{d,i}$ is the d-axis synchronous reactance minus transient reactance, and $q_{\ell,i}$ is the reactive power consumption. Eq. (3) describes the swing equation model of active power exchange between node i and neighboring¹ nodes $j \in \mathcal{N}_i$. With the internal matching controller from [16], [17], the dynamics of the \mathcal{I} nodes can be described in an analogous way as change of the angular momentum L_i of a virtual oscillator with a virtual damping coefficient $A_i > 0$. Eq. (4) models the transient dynamics of voltage magnitudes U_i of \mathcal{G} nodes, and (5)–(6) describe the active and reactive power conservation at \mathcal{L} nodes. The sending-end active and reactive power flows p_i and q_i in (3)–(6) are evaluated by the lossy AC power flow equations [19]

$$p_i = \sum_{j \in \mathcal{N}_i} B_{ij} U_i U_j \sin(\vartheta_{ij}) + G_{ii} U_i^2 + \sum_{j \in \mathcal{N}_i} G_{ij} U_i U_j \cos(\vartheta_{ij}), \quad i \in \mathcal{V}, \quad (7)$$

$$q_i = - \sum_{j \in \mathcal{N}_i} B_{ij} U_i U_j \cos(\vartheta_{ij}) + B_{ii} U_i^2 + \sum_{j \in \mathcal{N}_i} G_{ij} U_i U_j \sin(\vartheta_{ij}), \quad i \in \mathcal{V}, \quad (8)$$

where B_{ij} [G_{ij}] denotes the negative of the susceptance [conductance] of line $(i, j) \in \mathcal{E}_p$, $B_{ii} = -b_i - \sum_{j \in \mathcal{N}_i} B_{ij}$ denotes the self-susceptance at node $i \in \mathcal{V}$, and $G_{ii} = -g_i - \sum_{j \in \mathcal{N}_i} G_{ij}$ denotes the self-conductance at node $i \in \mathcal{V}$.

Within the model, the active power generations $p_{g,i}$, voltage magnitudes U_i of \mathcal{I} nodes and excitation voltages $U_{f,i}$ of \mathcal{G} nodes constitute the controlled input variables, whereas the active and reactive power consumptions $p_{\ell,i}$ and $q_{\ell,i}$ constitute the uncontrollable (i.e. disturbance) inputs of the network.

III. OPTIMIZATION PROBLEMS OF NETWORK PARTICIPANTS

Let $\mathcal{P} = \{1, \dots, |\mathcal{P}|\}$ denote the set of PPOs and $\mathcal{Z} = \{1, \dots, |\mathcal{Z}|\}$ be the set of CCs. As illustrated in Fig. 1, each node is associated to exactly one CC and each \mathcal{G} and \mathcal{I} node is associated to exactly one PPO. We note $i \in \mathcal{V}_{\pi}^{\mathcal{P}}$ if node i belongs to PPO $\pi \in \mathcal{P}$ and $i \in \mathcal{V}_k^{\mathcal{Z}}$ if node i belongs to CC $k \in \mathcal{Z}$.

A. Producers

Each PPO $\pi \in \mathcal{P}$ seeks to maximize its overall profit

$$P_{\pi} = \sum_{i \in \mathcal{V}_{\pi}^{\mathcal{P}}} P_{\pi,i} = \sum_{i \in \mathcal{V}_{\pi}^{\mathcal{P}}} -C_i(p_{g,i}) + \lambda_i \cdot p_{g,i} - \omega_i \cdot p_{g,i}, \quad (9)$$

¹The set \mathcal{N}_i contains all adjacent nodes of $i \in \mathcal{V}$ without consideration of the edge direction.

where $C_i(p_{g,i})$ is assumed to be a convex function representing the production costs at node i , λ_i is the local price for the active power generation $p_{g,i}$, and $-\omega_i \cdot p_{g,i}$ is an additive penalty for active power generation during an overfrequency period (or, respectively, an additive reward for active power generation during an underfrequency period).

Denote by $\mathbf{p}_{g,\pi}$, $\mathbf{U}_{f,\pi}$, and $\mathbf{U}_{\mathcal{I},\pi}$ the corresponding vectors of $p_{g,i}$, $U_{f,i}$, and $U_{\mathcal{I},i}$ associated to PPO $\pi \in \mathcal{P}$. The individual profit P_π in (9) is driven by the local prices λ_i , which are offered by the respective CC at node $i \in \mathcal{V}_\pi^P$. In addition, the flexibilities $\mathbf{p}_{g,\pi}$, $\mathbf{U}_{f,\pi}$, and $\mathbf{U}_{\mathcal{I},\pi}$ may be bounded from above or below². Accordingly, each PPO $\pi \in \mathcal{P}$ aims at solving the constrained optimization problem

$$\max_{\mathbf{p}_{g,\pi}, \mathbf{U}_{f,\pi}, \mathbf{U}_{\mathcal{I},\pi}} P_\pi \quad (10a)$$

$$\text{s.t.} \quad \underline{p}_{g,i} \leq p_{g,i} \leq \bar{p}_{g,i}, \quad i \in \mathcal{V}_\pi^P, \quad (10b)$$

$$\underline{U}_{f,i} \leq U_{f,i} \leq \bar{U}_{f,i} \quad i \in \mathcal{V}_\pi^P \cap \mathcal{V}_{\mathcal{G}}, \quad (10c)$$

$$\underline{U}_i \leq U_i \leq \bar{U}_i, \quad i \in \mathcal{V}_\pi^P \cap \mathcal{V}_{\mathcal{I}}. \quad (10d)$$

B. Consumers

Consumers at node $i \in \mathcal{V}$ are assumed to be inflexible and are characterized by a fixed active power consumption $p_{\ell,i}$. The cumulative cost for consumers in cell $k \in \mathcal{Z}$ is thus

$$C_k^\ell = \Lambda_k \cdot (\Phi_k + \sum_{i \in \mathcal{V}_k^Z} p_{\ell,i}), \quad (11)$$

where Λ_k denotes the cell specific electricity price and

$$\Phi_k = \sum_{i \in \mathcal{V}_k^Z} \left(G_{ii} U_i^2 + \sum_{j \in \mathcal{N}_i} G_{ij} U_i U_j \cos(\vartheta_{ij}) \right) \quad (12)$$

represents the resistive transmission losses within cell k .

C. Cell Coordinators

For all $i, j \in \mathcal{V}_k^Z$, the CC $k \in \mathcal{Z}$ seeks to choose the cell-specific price $\Lambda_k = \lambda_i = \lambda_j$ in such a way that the own utility function U_k (revenues from consumers minus payments to the PPOs) is maximized. Consequently, with

$$U_k = \Lambda_k \cdot \left(\Phi_k + \sum_{i \in \mathcal{V}_k^Z} p_{\ell,i} \right) - \Lambda_k \cdot \sum_{\substack{i \in \mathcal{V}_k^Z \\ i \notin \mathcal{V}_{\mathcal{L}}}} p_{g,i}, \quad (13)$$

each CC $k \in \mathcal{Z}$ aims to solve the optimization problem

$$\max_{\Lambda_k} U_k. \quad (14)$$

Following the lines of [2], we can use a distributed reformulation of (14) as follows:

$$\max_{\lambda_k} \sum_{i \in \mathcal{V}_k^Z} \left(\lambda_i \cdot (\varphi_i + p_{\ell,i}) \right) - \sum_{\substack{i \in \mathcal{V}_k^Z \\ i \notin \mathcal{V}_{\mathcal{L}}}} \lambda_i p_{g,i} \quad (15a)$$

$$\text{s.t.} \quad (\mathbf{D}_c^k)^\top \boldsymbol{\lambda}_k = \mathbf{0}, \quad (15b)$$

²It was shown in [18, Proposition 1] that upper [lower] bounds of U_i for \mathcal{G} nodes can be transformed into upper [lower] bounds of $U_{f,i}$ by a linear mapping.

where $\boldsymbol{\lambda}_k = \text{col}_{i \in \mathcal{V}_k^Z} \{\lambda_i\}$ and

$$\varphi_i = G_{ii} U_i^2 + \sum_{j \in \mathcal{N}_i} G_{ij} U_i U_j \cos(\vartheta_{ij}) \quad (16)$$

and \mathbf{D}_c^k is the incidence matrix of a connected communication graph $\mathcal{G}_c^k = (\mathcal{V}_k^Z, \mathcal{E}_c^k)$. The reformulation (15) of (14) is exact since $\Phi_k = \sum_{i \in \mathcal{V}_k^Z} \varphi_i$ and since (15b) holds if and only if for each cell $k \in \mathcal{Z}$, all nodal prices λ_i, λ_j with $i, j \in \mathcal{V}_k^Z$ are equal to a cell-specific price Λ_k .

D. Primal-Dual Gradient Controller

We now derive control laws for each network participant based on the optimization problems above. For PPO $\pi \in \mathcal{P}$, consider the Lagrangian of (10),

$$\begin{aligned} \mathcal{L}_\pi = & -P_\pi + \boldsymbol{\mu}_{p^-, \pi}^\top (\underline{\mathbf{p}}_{g,\pi} - \mathbf{p}_{g,\pi}) + \boldsymbol{\mu}_{p^+, \pi}^\top (\mathbf{p}_{g,\pi} - \bar{\mathbf{p}}_{g,\pi}) \\ & + \boldsymbol{\mu}_{\mathcal{G}^-, \pi}^\top (\underline{\mathbf{U}}_{f,\pi} - \mathbf{U}_{f,\pi}) + \boldsymbol{\mu}_{\mathcal{G}^+, \pi}^\top (\mathbf{U}_{f,\pi} - \bar{\mathbf{U}}_{f,\pi}) \\ & + \boldsymbol{\mu}_{\mathcal{I}^-, \pi}^\top (\underline{\mathbf{U}}_{\mathcal{I},\pi} - \mathbf{U}_{\mathcal{I},\pi}) + \boldsymbol{\mu}_{\mathcal{I}^+, \pi}^\top (\mathbf{U}_{\mathcal{I},\pi} - \bar{\mathbf{U}}_{\mathcal{I},\pi}), \end{aligned}$$

where $\boldsymbol{\mu}_{(\cdot), \pi}$ denotes the vectors of Lagrange multipliers for the inequality constraints (10b)–(10d). Since (10) is convex and Slater's Constraint Qualification [20] is fulfilled, the KKT conditions specifying a saddle point of \mathcal{L}_π can be applied to derive a necessary and sufficient condition for an optimizer $(\cdot)^*$ of (10):

$$0 = \nabla C_\pi(\mathbf{p}_{g,\pi}^*) - \boldsymbol{\lambda}_\pi + \boldsymbol{\omega}_\pi - \boldsymbol{\mu}_{g^-, \pi}^* + \boldsymbol{\mu}_{g^+, \pi}^*, \quad (17)$$

$$0 = -\boldsymbol{\mu}_{\mathcal{G}^-, \pi}^* + \boldsymbol{\mu}_{\mathcal{G}^+, \pi}^*, \quad (18)$$

$$0 = \boldsymbol{\mu}_{\mathcal{I}^-, \pi}^* - \boldsymbol{\mu}_{\mathcal{I}^+, \pi}^*, \quad (19)$$

$$0 = (\boldsymbol{\mu}_{g^-, \pi}^*)^\top (\underline{\mathbf{p}}_{g,\pi} - \mathbf{p}_{g,\pi}^*), \quad (20)$$

$$0 = (\boldsymbol{\mu}_{g^+, \pi}^*)^\top (\mathbf{p}_{g,\pi}^* - \bar{\mathbf{p}}_{g,\pi}), \quad (21)$$

$$0 = (\boldsymbol{\mu}_{\mathcal{G}^-, \pi}^*)^\top (\underline{\mathbf{U}}_{f,\pi} - \mathbf{U}_{f,\pi}^*), \quad (22)$$

$$0 = (\boldsymbol{\mu}_{\mathcal{G}^+, \pi}^*)^\top (\mathbf{U}_{f,\pi}^* - \bar{\mathbf{U}}_{f,\pi}), \quad (23)$$

$$0 = (\boldsymbol{\mu}_{\mathcal{I}^-, \pi}^*)^\top (\underline{\mathbf{U}}_{\mathcal{I},\pi} - \mathbf{U}_{\mathcal{I},\pi}^*), \quad (24)$$

$$0 = (\boldsymbol{\mu}_{\mathcal{I}^+, \pi}^*)^\top (\mathbf{U}_{\mathcal{I},\pi}^* - \bar{\mathbf{U}}_{\mathcal{I},\pi}), \quad (25)$$

$$0 \leq \boldsymbol{\mu}_{\mathcal{G}^-, \pi}^*, \boldsymbol{\mu}_{\mathcal{G}^+, \pi}^*, \boldsymbol{\mu}_{\mathcal{I}^-, \pi}^*, \boldsymbol{\mu}_{\mathcal{I}^+, \pi}^*, \boldsymbol{\mu}_{g^-, \pi}^*, \boldsymbol{\mu}_{g^+, \pi}^*, \quad (26)$$

where $\nabla C_\pi(\mathbf{p}_{g,\pi}) = \text{diag}_{i \in \mathcal{V}_\pi^P} \{\nabla C_i(p_{g,i})\}$. Application of the primal-dual gradient method [21] leads to the following controller equations:

$$\boldsymbol{\tau}_{g,\pi} \dot{\mathbf{p}}_{g,\pi} = -\nabla C_\pi(\mathbf{p}_{g,\pi}) + \boldsymbol{\lambda}_\pi - \boldsymbol{\omega}_\pi + \boldsymbol{\mu}_{g^-, \pi} - \boldsymbol{\mu}_{g^+, \pi}, \quad (27)$$

$$\boldsymbol{\tau}_{\mathcal{G},\pi} \dot{\mathbf{U}}_{f,\pi} = \boldsymbol{\mu}_{\mathcal{G}^-, \pi} - \boldsymbol{\mu}_{\mathcal{G}^+, \pi}, \quad (28)$$

$$\boldsymbol{\tau}_{\mathcal{I},\pi} \dot{\mathbf{U}}_{\mathcal{I},\pi} = -\boldsymbol{\mu}_{\mathcal{I}^-, \pi} + \boldsymbol{\mu}_{\mathcal{I}^+, \pi}, \quad (29)$$

$$\boldsymbol{\tau}_{\boldsymbol{\mu}_{g^-, \pi}} \dot{\boldsymbol{\mu}}_{g^-, \pi} = \langle \underline{\mathbf{p}}_{g,\pi} - \mathbf{p}_{g,\pi} \rangle_{\boldsymbol{\mu}_{g^-, \pi}}^+, \quad (30)$$

$$\boldsymbol{\tau}_{\boldsymbol{\mu}_{g^+, \pi}} \dot{\boldsymbol{\mu}}_{g^+, \pi} = \langle \mathbf{p}_{g,\pi} - \bar{\mathbf{p}}_{g,\pi} \rangle_{\boldsymbol{\mu}_{g^+, \pi}}^+, \quad (31)$$

$$\boldsymbol{\tau}_{\boldsymbol{\mu}_{\mathcal{G}^-, \pi}} \dot{\boldsymbol{\mu}}_{\mathcal{G}^-, \pi} = \langle \underline{\mathbf{U}}_{f,\pi} - \mathbf{U}_{f,\pi} \rangle_{\boldsymbol{\mu}_{\mathcal{G}^-, \pi}}^+, \quad (32)$$

$$\boldsymbol{\tau}_{\boldsymbol{\mu}_{\mathcal{G}^+, \pi}} \dot{\boldsymbol{\mu}}_{\mathcal{G}^+, \pi} = \langle \mathbf{U}_{f,\pi} - \bar{\mathbf{U}}_{f,\pi} \rangle_{\boldsymbol{\mu}_{\mathcal{G}^+, \pi}}^+, \quad (33)$$

$$\boldsymbol{\tau}_{\boldsymbol{\mu}_{\mathcal{I}^-, \pi}} \dot{\boldsymbol{\mu}}_{\mathcal{I}^-, \pi} = \langle \underline{\mathbf{U}}_{\mathcal{I},\pi} - \mathbf{U}_{\mathcal{I},\pi} \rangle_{\boldsymbol{\mu}_{\mathcal{I}^-, \pi}}^+, \quad (34)$$

$$\boldsymbol{\tau}_{\boldsymbol{\mu}_{\mathcal{I}^+, \pi}} \dot{\boldsymbol{\mu}}_{\mathcal{I}^+, \pi} = \langle \mathbf{U}_{\mathcal{I},\pi} - \bar{\mathbf{U}}_{\mathcal{I},\pi} \rangle_{\boldsymbol{\mu}_{\mathcal{I}^+, \pi}}^+. \quad (35)$$

with diagonal matrices $\tau_{(\cdot)} \succ 0$. The Lagrangian of (15) equals

$$\mathcal{L}_k^* = - \sum_{i \in \mathcal{V}_k^z} (\lambda_i \cdot (\varphi_i + p_{\ell,i})) + \sum_{\substack{i \in \mathcal{V}_k^z \\ i \notin \mathcal{V}_c}} \lambda_i p_{g,i} + \nu_k^\top (D_c^k)^\top \lambda_k,$$

where ν_k is the Lagrange multiplier associated to the linear equality constraint (15b). Since (14) is convex and Slater's Constraint Qualification is fulfilled, we can again specify the KKT conditions

$$0 = \mathbf{p}_{g,k} - \varphi_k - \mathbf{p}_{\ell,k} + D_c^k \nu_k^*, \quad (36)$$

$$0 = (D_c^k)^\top \lambda_k^*. \quad (37)$$

Application of the primal-dual gradient method yields

$$\tau_{\lambda,k} \dot{\lambda}_k = -\mathbf{p}_{g,k} + \varphi_k + \mathbf{p}_{\ell,k} - D_c^k \nu_k, \quad (38)$$

$$\tau_{\nu,k} \dot{\nu}_k = (D_c^k)^\top \lambda_k. \quad (39)$$

The simultaneous execution of the optimization schemes of PPOs $\pi \in \mathcal{P}$ and CCs $k \in \mathcal{Z}$ leads to a superposition of the derived control equations (27)–(35), (38)–(39). Consequently, the resulting closed-loop system consists of the physical system (2)–(8) together with the controller equations

$$\tau_g \dot{\mathbf{p}}_g = -\nabla \mathcal{C}(\mathbf{p}_g) + \lambda - \omega + \mu_{g-} - \mu_{g+}, \quad (40)$$

$$\tau_{U_g} \dot{U}_f = \mu_{g-} - \mu_{g+}, \quad (41)$$

$$\tau_{U_I} \dot{U}_I = -\mu_{I-} + \mu_{I+}, \quad (42)$$

$$\tau_{\mu_{g-}} \dot{\mu}_{g-} = \langle \underline{\mathbf{p}}_g - \mathbf{p}_g \rangle_{\mu_{g-}}^+, \quad (43)$$

$$\tau_{\mu_{g+}} \dot{\mu}_{g+} = \langle \mathbf{p}_g - \bar{\mathbf{p}}_g \rangle_{\mu_{g+}}^+, \quad (44)$$

$$\tau_{\mu_{g-}} \dot{\mu}_{g-} = \langle \underline{U}_f - U_f \rangle_{\mu_{g-}}^+, \quad (45)$$

$$\tau_{\mu_{g+}} \dot{\mu}_{g+} = \langle U_f - \bar{U}_f \rangle_{\mu_{g+}}^+, \quad (46)$$

$$\tau_{\mu_{I-}} \dot{\mu}_{I-} = \langle \underline{U}_I - U_I \rangle_{\mu_{I-}}^+, \quad (47)$$

$$\tau_{\mu_{I+}} \dot{\mu}_{I+} = \langle U_I - \bar{U}_I \rangle_{\mu_{I+}}^+, \quad (48)$$

$$\tau_{\lambda} \dot{\lambda} = -\mathbf{p}_g + \varphi + \mathbf{p}_{\ell} - D_c \nu, \quad (49)$$

$$\tau_{\nu} \dot{\nu} = D_c^\top \lambda, \quad (50)$$

where the parameters and variables in (40)–(50) are stacked vectors or diagonal matrices of appropriate sizes for all $\pi \in \mathcal{P}$ and $k \in \mathcal{Z}$, e.g. $\tau_g = \text{diag}_{\pi \in \mathcal{P}} \{\tau_{g,\pi}\}$ and $D_c = \text{col}_{k \in \mathcal{Z}} \{D_c^k\}$, and $\mathcal{C}(\mathbf{p}_g)$ equals the sum of all cost functions $\mathcal{C}_\pi(\mathbf{p}_g, \pi)$ in (9).

Remark 1: Note that D_c has a block diagonal structure, thus the corresponding communication graph \mathcal{G}_c is disconnected and contains $|\mathcal{Z}|$ connected subgraphs.

Before discussing the interactions of cell-specific prices, we point out a key result concerning the zero-frequency deviation of the closed-loop system (2)–(8), (40)–(50):

Proposition 1 (Zero Frequency Deviation): At each equilibrium of (2)–(8), (40)–(50), it holds that $\omega_i = 0$ for all $i \in \mathcal{V}$, i.e. each node is operating at the nominal frequency.

Proof: Eq. (2) can be written in vector-matrix notation as $\dot{\mathbf{v}} = D_p^\top \omega$, where D_p denotes the incidence matrix of the physical network \mathcal{G}_p . Since \mathcal{G}_p is a connected graph, each equilibrium ω^* with $0 = D_p^\top \omega^*$ fulfills $\omega^* = \omega^* \cdot \mathbb{1}$, i.e. the nodal frequencies are synchronized at steady state. Since

$\mathbb{1}^\top \varphi = \Phi$ and $\mathbb{1}^\top D_c = 0$, left-multiplying (49) by $\mathbb{1}^\top$ and inserting the equilibrium values implies

$$0 = - \sum_{i \in \mathcal{V}_G \cup \mathcal{V}_Z} p_{g,i}^* + \sum_{i \in \mathcal{V}} p_{\ell,i} + \Phi. \quad (51)$$

Due to the fact that $\Phi = \sum_{i \in \mathcal{V}} p_i$, a summation of all equations in (3) and (5) and insertion of the equilibrium values leads to

$$0 = - \sum_{i \in \mathcal{V}_G \cup \mathcal{V}_Z} A_i \omega_i^* + \sum_{i \in \mathcal{V}_G \cup \mathcal{V}_Z} p_{g,i}^* - \sum_{i \in \mathcal{V}} p_{\ell,i} - \Phi. \quad (52)$$

Comparison between (51) and (52) yields

$$0 = - \sum_{i \in \mathcal{V}_G \cup \mathcal{V}_Z} A_i \omega_i^* = -\omega^* \cdot \sum_{i \in \mathcal{V}_G \cup \mathcal{V}_Z} A_i. \quad (53)$$

Finally, since $A_i > 0$ holds by definition, it follows that ω^* is zero. ■

IV. INTERACTION BETWEEN ENERGY CELLS

Equation (50) implies that at each equilibrium of (40)–(50), nodal prices $\lambda_i, \lambda_j \in \mathcal{V}_k^z$ are equal to a common zonal price Λ_k for each cell $k \in \mathcal{Z}$. This allows to set incentives for increased or decreased power generation by means of differences in zonal prices. However, Remark 1 implies that there is no direct relationship between individual Λ_k .

A. Coupling of zonal prices Λ_k

To provide interdependencies between the zonal prices, we may impose additional constraints of the form

$$\lambda_i \stackrel{!}{=} \eta_{ij} \cdot \lambda_j, \quad (54)$$

for pairs of nodes $i, j \in \mathcal{V}$, which are located in *different* cells, where $\eta_{ij} > 0$ is an appropriate multiplier. If (15b) is extended by these additional constraints (54), both (15b) and (54) can be combined to the extended constraint

$$0 = (D_c^+)^T \lambda. \quad (55)$$

Hence, the resulting controller equations (49)–(50) become

$$\tau_{\lambda} \dot{\lambda} = -\mathbf{p}_g + \varphi + \mathbf{p}_{\ell} - D_c^+ \nu, \quad (56)$$

$$\tau_{\nu} \dot{\nu} = (D_c^+)^T \lambda. \quad (57)$$

With this notation, D_c^+ can be interpreted as the incidence matrix of an extended, weighted communication graph $\mathcal{G}_c^+ = (\mathcal{V}, (\mathcal{E}_c, \mathcal{E}_c^b))$, where \mathcal{E}_c^b represents communication across cell boundaries. The weights of the edges of \mathcal{G}_c^+ are equal to η_{ij} , if the two adjacent nodes belong to different cells, and equal to 1 if i and j are located in the same cell.

Assumption 1: The multipliers η_{ij} are chosen in a *feasible* sense such that there exists at least one $\lambda > 0_n$ fulfilling (55). In this case, each cell $k \in \mathcal{Z}$ can be characterized with a specific participation factor $\kappa_k > 0$ such that each η_{ij} is calculated by $\eta_{ij} = \kappa_{k_1} / \kappa_{k_2}$ if i is located in cell k_1 and j is located in cell k_2 .

Proposition 2 (Connectivity of Zonal Prices): If \mathcal{G}_c^+ is weakly connected, then

$$\frac{\lambda_1}{\kappa_{k_1}} = \frac{\lambda_2}{\kappa_{k_2}} = \dots = \frac{\lambda_n}{\kappa_{k_n}} =: \Lambda^\circ, \quad (58)$$

where κ_{k_i} denotes the corresponding participation factor belonging to the cell k where node $i \in \mathcal{V}$ is located.

Proof: Define the auxiliary matrices $\mathbf{K}_1 = \text{diag}_{ij \in (\mathcal{E}_c, \mathcal{E}_c^b)} \{\eta_{ij}\} \succ 0$ and $\mathbf{K}_2 = \text{diag}_{i \in \mathcal{V}} \{\kappa_{k_i}\} \succ 0$. Then, $(\mathbf{D}_c^+)^{\top} \boldsymbol{\lambda} = \mathbf{0}$ is equivalent to

$$\underbrace{\mathbf{K}_1^{-1} \mathbf{0}}_0 = \mathbf{K}_1^{-1} (\mathbf{D}_c^+)^{\top} \boldsymbol{\lambda} = \underbrace{\mathbf{K}_1^{-1} (\mathbf{D}_c^+)^{\top} \mathbf{K}_2}_{=:(\mathbf{D}_c^{\circ})^{\top}} \underbrace{\mathbf{K}_2^{-1} \boldsymbol{\lambda}}_{=:\boldsymbol{\lambda}^{\circ}}. \quad (59)$$

Inserting the definition of \mathbf{K}_1 into (59) with $\eta_{ij} = \kappa_{k_1}/\kappa_{k_2}$ reveals that \mathbf{D}_c° is the incidence matrix of a new communication graph \mathcal{G}_c° , which is equivalent to \mathcal{G}_c^+ with all edge weights set to 1. Thus each solution $\boldsymbol{\lambda}^{\circ}$ of the resulting equation $\mathbf{0} = (\mathbf{D}_c^{\circ})^{\top} \boldsymbol{\lambda}^{\circ}$ is of the form $\boldsymbol{\lambda}^{\circ} = \mathbf{1} \cdot \text{const}$, i.e. each component of $\boldsymbol{\lambda}^{\circ}$ has the same value. Finally, since $\boldsymbol{\lambda}^{\circ} = \mathbf{K}_2^{-1} \boldsymbol{\lambda} = \text{col}_{i \in \mathcal{V}} \{\lambda_i/\kappa_{k_i}\}$, this leads to (58). ■

Remark 2: If \mathcal{G}_c^+ is not weakly connected, then (58) holds separately for all nodes in each weakly connected component in \mathcal{G}_c^+ .

Remark 3: The uniform price Λ° resulting when $\kappa = \mathbf{1}$ is called the *market-clearing price* of the network, since in this case the total revenue of all PPOs is equal to the cumulative costs of all CCs and consumers. Accordingly, κ_k describes the multiplicity of the cell-specific price Λ_k compared to Λ° .

In the following, we will discuss to what extent κ can be applied to modify the impact of specific cells on the overall network. For this purpose, we first investigate the equivalence of the multi-objective problem of PPOs and CCs to a modified, centralized optimization problem.

B. Comparison with Centralized Optimization

Proposition 3 (Equivalence to Centralized Optimization): Define the centralized optimization problem

$$\max_{\mathbf{p}_g, \mathbf{U}_f, \mathbf{U}_{\mathcal{I}}} \mathbf{P}^{\kappa} \quad (60a)$$

$$\text{s.t. } \boldsymbol{\Phi} = \sum_{i \in \mathcal{V}_g \cup \mathcal{V}_{\mathcal{I}}} p_{g,i} - \sum_{i \in \mathcal{V}} p_{\ell,i}, \quad (60b)$$

$$\underline{\mathbf{p}}_g \leq \mathbf{p}_g \leq \overline{\mathbf{p}}_g, \quad (60c)$$

$$\underline{\mathbf{U}}_f \leq \mathbf{U}_f \leq \overline{\mathbf{U}}_f, \quad (60d)$$

$$\underline{\mathbf{U}}_{\mathcal{I}} \leq \mathbf{U}_{\mathcal{I}} \leq \overline{\mathbf{U}}_{\mathcal{I}}, \quad (60e)$$

where

$$\mathbf{P}^{\kappa} = - \sum_{k \in \mathcal{Z}} \sum_{i \in \mathcal{V}_k^z} \frac{1}{\kappa_k} \cdot \mathbf{C}_i(p_{g,i}) - \sum_{i \in \mathcal{V}_g \cup \mathcal{V}_{\mathcal{I}}} \omega_i \cdot p_{g,i}. \quad (61)$$

Then each optimizer $(\mathbf{p}_g^*, \mathbf{U}_f^*, \mathbf{U}_{\mathcal{I}}^*)$ of (60) is an equilibrium of (40)–(48), (56)–(57) and vice versa. If $\mathbf{C}_i(p_{g,i})$ in (61) are strictly convex, then $(\mathbf{p}_g^*, \mathbf{U}_f^*, \mathbf{U}_{\mathcal{I}}^*)$ is unique.

Proof: Constraint (60b) is equivalent to (cf. [2, p. 2615])

$$\widehat{\mathbf{D}}_c \widehat{\boldsymbol{\nu}} = \mathbf{p}_g - \mathbf{p}_{\ell} - \boldsymbol{\varphi}, \quad (62)$$

where $\boldsymbol{\varphi} = \text{col}_i \{\varphi_i\}$ (see (16)) and $\widehat{\mathbf{D}}_c$ is the incidence matrix of a connected communication graph. If we choose $\widehat{\mathbf{D}}_c = \mathbf{D}_c^{\circ}$

and define $\mathbf{C}^{\kappa}(\mathbf{p}_g) = \sum_{k \in \mathcal{Z}} \sum_{i \in \mathcal{V}_k^z} \frac{1}{\kappa_k} \cdot \mathbf{C}_i(p_{g,i})$, then the Lagrangian of (60) becomes

$$\begin{aligned} \mathcal{L}^{\kappa} &= \mathbf{C}^{\kappa}(\mathbf{p}_g) + \sum_{i \in \mathcal{V}_g \cup \mathcal{V}_{\mathcal{I}}} \omega_i \cdot p_{g,i} \\ &+ \widehat{\boldsymbol{\lambda}}^{\top} (\mathbf{D}_c^{\circ} \widehat{\boldsymbol{\nu}} - \mathbf{p}_g + \mathbf{p}_{\ell} + \boldsymbol{\varphi}) \\ &+ \widehat{\boldsymbol{\mu}}_{g-}^{\top} (\underline{\mathbf{p}}_g - \mathbf{p}_g) + \widehat{\boldsymbol{\mu}}_{g+}^{\top} (\mathbf{p}_g - \overline{\mathbf{p}}_g) \\ &+ \widehat{\boldsymbol{\mu}}_{\mathcal{I}-}^{\top} (\underline{\mathbf{U}}_f - \mathbf{U}_f) + \widehat{\boldsymbol{\mu}}_{\mathcal{I}+}^{\top} (\mathbf{U}_f - \overline{\mathbf{U}}_f) \\ &+ \widehat{\boldsymbol{\mu}}_{\mathcal{I}-}^{\top} (\underline{\mathbf{U}}_{\mathcal{I}} - \mathbf{U}_{\mathcal{I}}) + \widehat{\boldsymbol{\mu}}_{\mathcal{I}+}^{\top} (\mathbf{U}_{\mathcal{I}} - \overline{\mathbf{U}}_{\mathcal{I}}), \end{aligned} \quad (63)$$

where $\widehat{\boldsymbol{\lambda}}$ denotes the Lagrange multiplier for equality constraint (62) and $\widehat{\boldsymbol{\mu}}_{(\cdot)}$ are the Lagrange multipliers for the inequality constraints (60c)–(60e). Since (60) is convex and Slater's Constraint Qualification is fulfilled, the primal-dual optimizer $(\cdot)^{\#}$ of (60) is given by

$$\mathbf{0} = -\nabla \mathbf{C}^{\kappa}(\mathbf{p}_g^{\#}) - \boldsymbol{\omega}_i + \widehat{\boldsymbol{\lambda}}^{\#} + \widehat{\boldsymbol{\mu}}_{g-}^{\#} - \widehat{\boldsymbol{\mu}}_{g+}^{\#}, \quad (64)$$

$$\mathbf{0} = \widehat{\boldsymbol{\mu}}_{g-}^{\#} - \widehat{\boldsymbol{\mu}}_{g+}^{\#}, \quad (65)$$

$$\mathbf{0} = -\widehat{\boldsymbol{\mu}}_{\mathcal{I}-}^{\#} + \widehat{\boldsymbol{\mu}}_{\mathcal{I}+}^{\#}, \quad (66)$$

$$\mathbf{0} = (\widehat{\boldsymbol{\mu}}_{g-}^{\#})^{\top} (\mathbf{p}_g - \overline{\mathbf{p}}_g), \quad (67)$$

$$\mathbf{0} = (\widehat{\boldsymbol{\mu}}_{g+}^{\#})^{\top} (\mathbf{p}_g^{\#} - \underline{\mathbf{p}}_g), \quad (68)$$

$$\mathbf{0} = (\widehat{\boldsymbol{\mu}}_{\mathcal{I}-}^{\#})^{\top} (\mathbf{U}_f - \overline{\mathbf{U}}_f), \quad (69)$$

$$\mathbf{0} = (\widehat{\boldsymbol{\mu}}_{\mathcal{I}+}^{\#})^{\top} (\mathbf{U}_f^{\#} - \underline{\mathbf{U}}_f), \quad (70)$$

$$\mathbf{0} = (\widehat{\boldsymbol{\mu}}_{\mathcal{I}-}^{\#})^{\top} (\mathbf{U}_{\mathcal{I}} - \overline{\mathbf{U}}_{\mathcal{I}}), \quad (71)$$

$$\mathbf{0} = (\widehat{\boldsymbol{\mu}}_{\mathcal{I}+}^{\#})^{\top} (\mathbf{U}_{\mathcal{I}}^{\#} - \underline{\mathbf{U}}_{\mathcal{I}}), \quad (72)$$

$$\mathbf{0} = -\mathbf{p}_g^{\#} + \boldsymbol{\varphi} + \mathbf{p}_{\ell} - \mathbf{D}_c^{\circ} \widehat{\boldsymbol{\nu}}^{\#}, \quad (73)$$

$$\mathbf{0} = (\mathbf{D}_c^{\circ})^{\top} \widehat{\boldsymbol{\lambda}}^{\#}, \quad (74)$$

$$\mathbf{0} \leq \boldsymbol{\mu}_{g-}^{\#}, \boldsymbol{\mu}_{g+}^{\#}, \boldsymbol{\mu}_{\mathcal{I}-}^{\#}, \boldsymbol{\mu}_{\mathcal{I}+}^{\#}, \boldsymbol{\mu}_{g-}^{\#}, \boldsymbol{\mu}_{g+}^{\#}. \quad (75)$$

Inserting the definition (59) in (74) and comparing with the right-hand side of (50) yields $\widehat{\boldsymbol{\lambda}}^{\#} = \mathbf{K}_2^{-1} \boldsymbol{\lambda}^*$. Hence with $\nabla \mathbf{C}^{\kappa}(\mathbf{p}_g^{\#}) = \mathbf{K}_2^{-1} \nabla \mathbf{C}(\mathbf{p}_g)$ in (64) and by comparing (64)–(75) with (40)–(50) we get the equivalences $\mathbf{p}_g^{\#} = \mathbf{p}_g^*$, $\mathbf{U}_f^{\#} = \mathbf{U}_f^*$, $\mathbf{U}_{\mathcal{I}}^{\#} = \mathbf{U}_{\mathcal{I}}^*$, $\widehat{\boldsymbol{\mu}}_{g-}^{\#} = \mathbf{K}_2^{-1} \boldsymbol{\mu}_{g-}^*$, $\widehat{\boldsymbol{\mu}}_{g+}^{\#} = \mathbf{K}_2^{-1} \boldsymbol{\mu}_{g+}^*$, $\widehat{\boldsymbol{\mu}}_{\mathcal{I}-}^{\#} = \boldsymbol{\mu}_{\mathcal{I}-}^*$, $\widehat{\boldsymbol{\mu}}_{\mathcal{I}+}^{\#} = \boldsymbol{\mu}_{\mathcal{I}+}^*$. Moreover, the dual optimizer $\boldsymbol{\nu}^*$ in (49) and the primal optimizer $\widehat{\boldsymbol{\nu}}^{\#}$ of (62) are connected via the relationship

$$-\mathbf{D}_c^{\circ} \boldsymbol{\nu}^{\#} + \mathbf{D}_c^+ \boldsymbol{\nu}^{\#} = \mathbf{0}. \quad (76)$$

From (59) it follows that $\mathbf{D}_c^{\circ} = \mathbf{K}_2 \mathbf{D}_c^+ \mathbf{K}_1^{-1}$ with $\mathbf{K}_1, \mathbf{K}_2 \succ 0$, thus the images of \mathbf{D}_c^+ and \mathbf{D}_c° are identical. Accordingly, for each $\boldsymbol{\lambda}^*$ there exists a $\widehat{\boldsymbol{\lambda}}^{\#}$ fulfilling (76), and vice versa.

In summary, for each primal-dual optimizer of (60) there exists exactly one corresponding equilibrium of (40)–(48), (56)–(57). In particular, $(\mathbf{p}_g^{\#}, \mathbf{U}_f^{\#}, \mathbf{U}_{\mathcal{I}}^{\#}) = (\mathbf{p}_g^*, \mathbf{U}_f^*, \mathbf{U}_{\mathcal{I}}^*)$. Since (60) is a convex optimization problem, convergence of the trajectory $(\mathbf{p}_g(t), \mathbf{U}_f(t), \mathbf{U}_{\mathcal{I}}(t))$ to $(\mathbf{p}_g^*, \mathbf{U}_f^*, \mathbf{U}_{\mathcal{I}}^*)$ is guaranteed (cf. [22, Theorem 2]).

If the cost functions $\mathbf{C}_i(p_{g,i})$ are strictly convex, then \mathbf{P}^{κ} is strictly concave. Hence, the equilibrium $(\mathbf{p}_g^{\#}, \mathbf{U}_f^{\#}, \mathbf{U}_{\mathcal{I}}^{\#})$ from centralized optimization and therewith the equilibrium $(\mathbf{p}_g^*, \mathbf{U}_f^*, \mathbf{U}_{\mathcal{I}}^*)$ from distributed optimization are unique. ■

C. Analysis of Pareto Efficiency

As stated in Proposition 3, the interaction of distributed PPOs and CCs, subject to cell-specific pricing by κ_k , leads to the same equilibrium $(\mathbf{p}_g, \mathbf{U}_f, \mathbf{U}_\mathcal{I})$ as if a centralized authority with full knowledge of the whole network would solve the optimization problem (60) with modified cost $\mathbf{C}^\kappa(\mathbf{p}_g)$, where the cumulative cost functions of each cell $k \in \mathcal{Z}$ are divided by κ_k . This equivalence reveals some further key properties of the distributed WoC controller that allow the evaluation of the Pareto efficiency of the equilibrium from a multi-objective perspective.

Remark 4: If $\kappa = \mathbf{1}$, then the objective function of (60) is

$$\mathbf{P}^\kappa = \sum_{\pi \in \mathcal{P}} \mathbf{P}^\pi - \sum_{k \in \mathcal{Z}} \mathbf{C}_k^\ell + \sum_{k \in \mathcal{Z}} \mathbf{U}_k = - \sum_{i \in \mathcal{V}} \mathbf{C}_i(p_i), \quad (77)$$

and thus equal to the sum of all payoffs of PPOs (9), consumers (11), and CCs (13). Accordingly, the distributed controller (40)–(48), (56)–(57) leads to a constrained minimization of the overall costs of power production.

As mentioned earlier, the participation factor κ_k can be used to increase (large κ_k) or decrease (small κ_k) the proportion of active power generation in cell $k \in \mathcal{Z}$ as compared to the other cells. It directly follows from Proposition 3 that the result of the optimization procedure (60) is invariant with respect to a scalar multiplication of κ , thus the level of excess or shortage of generation in cell k does not depend on the absolute value of κ_k , but on the relative value compared to the other components in κ .

Besides the fact that all $\kappa > \mathbf{0}$ are feasible (cf. Assumption 1), it has to be stressed that each κ achieves an *efficient* allocation in the sense that for a given $\kappa' > \mathbf{0}$, there is no possibility to find a “better” $\kappa'' \neq \kappa'$, $\kappa'' > \mathbf{0}$ such that at least one cell is at lower cost and no cell is at higher cost. This is formalized in the next proposition.

Proposition 4 (Pareto efficiency of κ): Define by

$$\mathbf{C}_k^{\text{total}} = - \left(\sum_{i \in \mathcal{V}_k^{\mathcal{Z}}} \sum_{\pi \in \mathcal{P}} \mathbf{P}_i^\pi \right) + \mathbf{C}_k^\ell - \mathbf{U}_k \quad (78)$$

the net costs of all network participants in cell $k \in \mathcal{Z}$. Consider the cost minimization problems summarizing the optimization problems³ of all network participants in cell k :

$$\min_{\mathbf{p}_{g,k}, \mathbf{U}_{f,k}, \mathbf{U}_{\mathcal{I},k}} \mathbf{C}_k^{\text{total}} \quad (79a)$$

$$\text{s.t.} \quad (\mathbf{D}_c^{k+})^\top \boldsymbol{\lambda}_k = \mathbf{0}, \quad (79b)$$

$$\underline{\mathbf{p}}_{g,k} \leq \mathbf{p}_{g,k} \leq \bar{\mathbf{p}}_{g,k}, \quad (79c)$$

$$\underline{\mathbf{U}}_{f,k} \leq \mathbf{U}_{f,k} \leq \bar{\mathbf{U}}_{f,k}, \quad (79d)$$

$$\underline{\mathbf{U}}_{\mathcal{I},k} \leq \mathbf{U}_{\mathcal{I},k} \leq \bar{\mathbf{U}}_{\mathcal{I},k}. \quad (79e)$$

Let $\kappa' > \mathbf{0}$ be fixed and denote by $\mathbf{C}_k^{\text{total}*}(\kappa')$ the corresponding value of $\mathbf{C}_k^{\text{total}}$ for an equilibrium of multi-objective problem (79) with parameter κ set to κ' . Then, there exists

³Eq. (79b) contains all elements of (55) that belong to nodes in cell k .

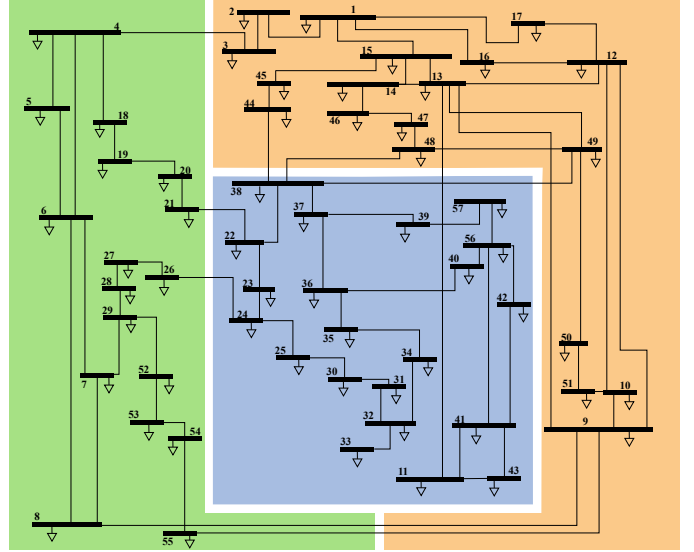


Fig. 2. IEEE 57-bus system divided into 3 cells [24].

TABLE I
ASSIGNMENT OF NODE TYPES

\mathcal{G}	2, 3, 6, 8, 9, 10, 19, 21, 29, 30, 32, 34, 37, 39, 40, 41, 44, 48, 55
\mathcal{I}	4, 11, 14, 15, 16, 17, 18, 22, 24, 25, 26, 33, 36, 42, 45, 46, 49, 50, 53
\mathcal{L}	1, 5, 7, 12, 13, 20, 23, 27, 28, 31, 35, 38, 43, 47, 51, 52, 54, 56, 57

no other *dominating* $\kappa'' > \mathbf{0}$ with $\kappa'' \neq \kappa'$ such that the following two conditions hold:

$$\forall k \in \mathcal{Z} : \quad \mathbf{C}_k^{\text{total}*}(\kappa'') \leq \mathbf{C}_k^{\text{total}*}(\kappa') \quad (80a)$$

$$\exists k \in \mathcal{Z} : \quad \mathbf{C}_k^{\text{total}*}(\kappa'') < \mathbf{C}_k^{\text{total}*}(\kappa') \quad (80b)$$

Proof: Taking into account that (79) are convex optimization problems and following the same lines as in the proof of Proposition 3, it can be shown that each KKT point of (79) is given by (64)–(75) and vice versa. For each $\kappa > \mathbf{0}$, the equivalent problem (60) is a linear scalarization of (79) with positive weights $1/\kappa_k > 0$. With [23, Proposition 9], it is implied that for each $\kappa' > \mathbf{0}$, the solution of (79) is a part of the Pareto front, hence there exists no $\kappa' > \mathbf{0}$ which is dominated by another $\kappa'' > \mathbf{0}$ in terms of (80). ■

V. CASE STUDY

We validate the performance of the developed distributed controller on the IEEE 57-bus test case, which is divided into three cells (see Fig. 2). The assignment to the node types is chosen equally distributed according to Table I.

A. Network Model and Parameterization

All of the following numerical values are given in p.u. with $U_{\text{base}} = 135$ kV and $S_{\text{base}} = 100$ MVA. The controller parameters $\tau_{\mu\mathcal{G}-}$, $\tau_{\mu\mathcal{G}+}$, and $\tau_{\mathbf{U}\mathcal{G}}$ are set to 0.01, while $\tau_{\mu\mathcal{I}+}$, $\tau_{\mu\mathcal{I}-}$, $\tau_{\mu\mathcal{G}+}$, and $\tau_{\mu\mathcal{G}-}$ are set to 0.001 and the other controller parameters in (40)–(50) are set to 0.1. The node parameters are chosen to be randomly distributed within the specific intervals in Table II. The lower and upper bounds of \mathbf{p}_g are set to $\underline{p}_{g,i} = -0.002$ and $\bar{p}_{g,i} = 0.003$ respectively, and the voltage limits are set to 0.98 and 1.02. At $t = 0$, the system is in synchronous mode with $\mathbf{L} = \mathbf{0}$ and all controller variables \mathbf{p}_g ,

TABLE II
NODE PARAMETERS

	A_i	M_i	$X_{d,i} - X'_{d,i}$	$\tau_{U,i}$
\mathcal{G}	[1.2; 1.7]	[20; 27]	[0.12; 0.19]	[6.4; 7.7]
\mathcal{I}	[1.2; 1.7]	[4; 5.5]	—	—
\mathcal{L}	[1.2; 1.7]	—	—	—

ν , λ , $\mu_{(\cdot)}$ are initialized to zero. Without loss of generality, we set $\mathcal{P} \equiv \mathcal{Z}$ and choose the cost functions to

$$c_{\pi}(\mathbf{p}_{\pi}) = \frac{1}{2} \cdot \left(\sum_{i \in \mathcal{V}_{\pi}^{\mathcal{P}}} \frac{1}{w_i} \cdot p_{g,i}^2 \right), \quad \pi \in \mathcal{P}, \quad (81)$$

where $w_i = 1 + 0.04 \cdot (i - 1)$. The initial values of ϑ_{ij} are chosen within the interval $[-0.04; 0.014]$ and all voltages U_i are chosen within the interval $[0.98; 1.02]$.

The active and reactive power consumptions \mathbf{p}_{ℓ} and \mathbf{q}_{ℓ} are piecewise constant in order to simulate a step change in generation or consumption in specific areas of the network. To this end, the initial values of \mathbf{p}_{ℓ} and \mathbf{q}_{ℓ} are chosen such that the AC power flow equations are satisfied. Subsequently, the following stepwise load increases or decreases are applied:

- at $t_1 = 1000$ s, the active power consumption $p_{\ell,28}$ in cell 3 increases by 0.1.
- at $t_2 = 3000$ s, the reactive power consumption $q_{\ell,28}$ at the same node increases by 0.1.
- at $t_3 = 5000$ s, two additional nodes, 20 and 27, which are also located in cell 3, increase both their active and reactive power consumption by 0.05.
- at $t_4 = 7000$ s, the power consumption of nodes 20, 27, and 28 is reset to their initial values. At the same time, active and reactive power consumption at load nodes 12, 13, and 43 in cells 1 and 2 increases by 0.05 each.
- at $t_5 = 9000$ s the active and reactive power consumptions of all above-mentioned nodes are multiplied by -1 to simulate a reversed load flow.

Let $D_{IEEE,57}$ denote the incidence matrix of the IEEE 57-bus test case and $D_{IEEE,57}^{-}$ denote the respective incidence matrix if all boundary edges of adjacent cells are removed. To investigate the role of connectivity of \mathcal{G}_p and \mathcal{G}_c and the effects of κ , we examine four different topological scenarios:

- 1) $D_p = D_{IEEE,57}$ and $D_c = D_{IEEE,57}^{-}$.
- 2) $D_p = D_c = D_{IEEE,57}$ with $\kappa = \mathbf{1}$.
- 3) $D_p = D_c = D_{IEEE,57}$ with $\kappa = [1 \ 5 \ 25]^{\top}$.
- 4) $D_p = D_c = D_{IEEE,57}^{-}$.

Scenario 4 is referred to as the *islanded* scenario without any physical or communication interconnection between cells.

B. Numerical Results

Fig. 3 shows the resulting active power generation $p_{g,i}$ at each node $i \in \mathcal{V}_{\mathcal{G}} \cup \mathcal{V}_{\mathcal{I}}$ for scenarios 1–4. It can be seen that the limits \underline{p}_g and \bar{p}_g are met and that, unless $p_{g,i}$ is at one of its limits, the individual share of active power generation for each cell is distributed proportional to the weighting factors w_i in (81). While the steps at 1000 s, 3000 s, and 5000 s (which are load steps in cell 3) have little impact on p_g in cells 1 and 2 for scenario 1 and no impact for the islanded scenario 4, the power sharing among individual cells is fixed for scenarios 2 and 3 and thus not dependent on the cell where the load step

occurs. In contrast, in scenarios 1 and 4 the contribution of the individual cells to meet the total consumption varies, with a considerably higher spread in scenario 4.

Analysis of the frequency (Fig. 4) and voltage curves⁴ reveals that in scenario 1, both frequency and voltage regulation is maintained at steady state, whereas scenario 4 shows an instable behavior after the third step⁵. For example, after the step at 5000 s, the increased consumption in cell 3 can no longer be covered by generators in the same cell, which results in a constant underfrequency of around 0.02 Hz. By contrast, the physical interconnection of the cells in scenario 1 allows compensation of the consumption by neighboring generators in cells 1 and 2 and thus a preservation of frequency at 50 Hz.

Fig. 5 gives a closer look at the varying courses of prices λ_i at all nodes $i \in \mathcal{V}$ for scenarios 1–3. In any of the scenarios, no price differences can be observed within each cell $k \in \{1, 2, 3\}$. This shows that the nodal prices have a very fast convergence to a cell-specific price Λ_k . While for scenarios 2 and 3, the relationship between cell-specific prices Λ_k is fixed according to the choice of κ , for scenario 1 the relationship changes after each step, depending on where the load step occurs.

VI. CONCLUSION

In this paper, we presented a distributed control strategy for dynamic pricing in zonal electricity markets. Incorporating the WoC concept, the interplay of different optimization problems of PPOs and CCs resulted in an overall control system for which frequency and voltage regulation as well as Pareto efficiency can be shown. Simulation studies on a modified IEEE 57-bus system compared different zonal pricing approaches with an islanded operation. The developed controller features low efforts for parameter tuning, since the choice of the free controller parameters $\tau_{(\cdot)}$ does not affect the value of the closed-loop equilibrium.

The remaining degrees of freedom manifest in a free choice of the participation factor $\kappa \in \mathbb{R}_{>0}^{|\mathcal{Z}|}$, which offers a sound perspective for deliberate over- or underweighting of PPOs in specific locations, while still preserving frequency and voltage stability as well as other operational constraints simultaneously. Future research will thus focus on superordinate control strategies for $\kappa(t)$ in order to create short-term and long-term incentives for power generation in areas where it is particularly needed.

REFERENCES

- [1] D. Feijer and F. Paganini, “Stability of primal–dual gradient dynamics and applications to network optimization,” *Automatica*, vol. 46, no. 12, pp. 1974–1981, 2010.
- [2] T. Stegink, C. D. Persis, and A. van der Schaft, “A unifying energy-based approach to stability of power grids with market dynamics,” *IEEE Transactions on Automatic Control*, vol. 62, no. 6, pp. 2612–2622, 2017.
- [3] E. Mallada, C. Zhao, and S. Low, “Optimal load-side control for frequency regulation in smart grids,” *IEEE Transactions on Automatic Control*, vol. 62, no. 12, pp. 6294–6309, 2017.

⁴The corresponding plot for the voltages verifies these results, but is omitted for reasons of space.

⁵The frequency plots for scenarios 2 and 3 are quite similar to scenario 1 and thus omitted for reasons of space.

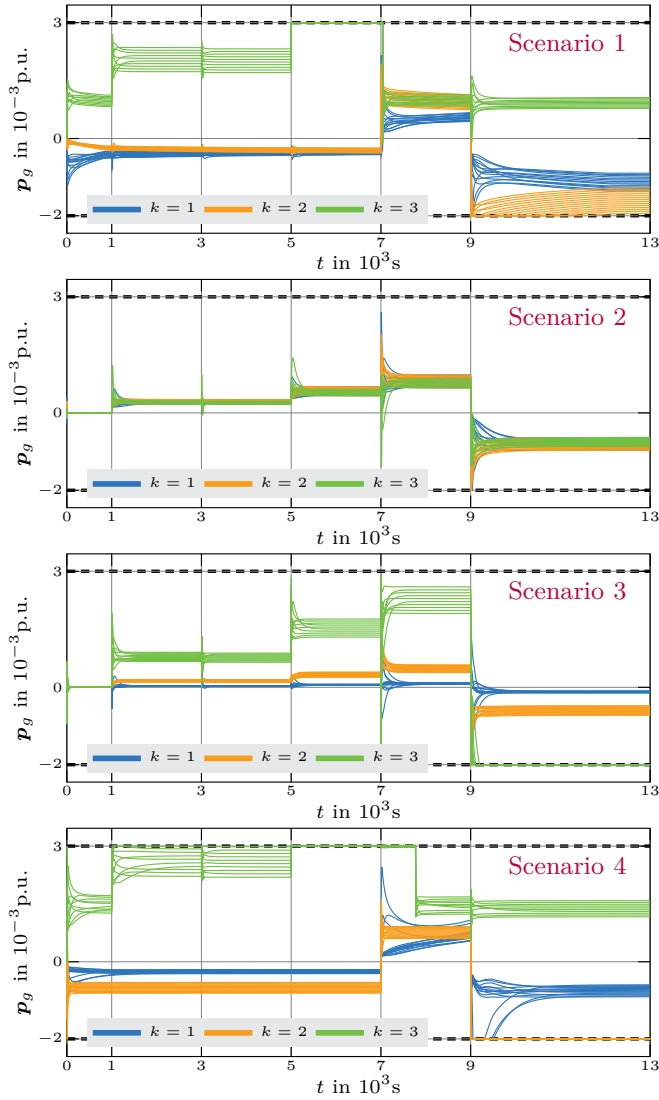


Fig. 3. Active power generations p_g for scenarios 1–4.

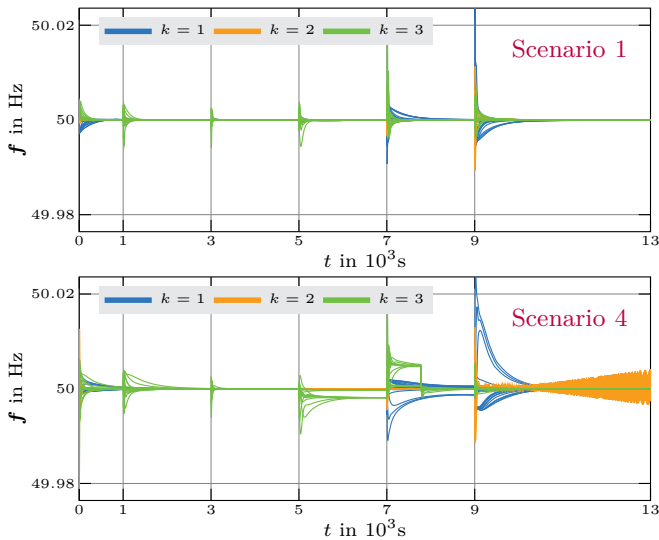


Fig. 4. Nodal frequencies f for scenarios 1 and 4.

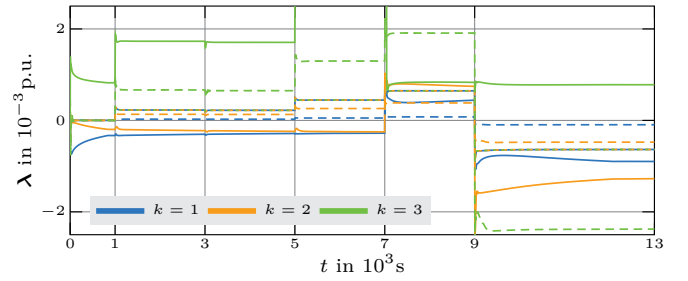


Fig. 5. Prices λ for scenario 1 (solid), 2 (dotted), and 3 (dashed).

- [4] F. Dörfler and S. Grammatico, “Gather-and-broadcast frequency control in power systems,” *Automatica*, vol. 79, pp. 296–305, 2017.
- [5] S. Magnússon, C. Fischione, and N. Li, “Voltage control using limited communication,” *IFAC-PapersOnLine*, vol. 50, no. 1, pp. 1–6, 2017.
- [6] X. Ma and N. Elia, “A distributed continuous-time gradient dynamics approach for the active power loss minimizations,” in *2013 51st Annual Allerton Conference on Communication, Control, and Computing (Allerton)*. IEEE, 2013, pp. 100–106.
- [7] X. Zhang and A. Papachristodoulou, “A real-time control framework for smart power networks: Design methodology and stability,” *Automatica*, vol. 58, pp. 43–50, 2015.
- [8] F. Dörfler, S. Bolognani, J. W. Simpson-Porco, and S. Grammatico, “Distributed control and optimization for autonomous power grids,” in *2019 18th European Control Conference (ECC)*. IEEE, 2019, pp. 2436–2453.
- [9] H. Liu, L. Tesfatsion, and A. A. Chowdhury, “Locational marginal pricing basics for restructured wholesale power markets,” in *2009 IEEE Power & Energy Society General Meeting*. IEEE, 2009, pp. 1–8.
- [10] D. K. Molzahn, F. Dörfler, H. Sandberg, S. H. Low, S. Chakrabarti, R. Baldick, and J. Lavaei, “A survey of distributed optimization and control algorithms for electric power systems,” *IEEE Transactions on Smart Grid*, vol. 8, no. 6, pp. 2941–2962, 2017.
- [11] T. Stegink, A. Cherukuri, C. D. Persis, A. van der Schaft, and J. Cortes, “Hybrid interconnection of iterative bidding and power network dynamics for frequency regulation and optimal dispatch,” *IEEE Transactions on Control of Network Systems*, vol. 6, no. 2, pp. 572–585, 2019.
- [12] A. Cherukuri, T. W. Stegink, C. D. Persis, Arjan J. van der Schaft, and J. Cortés, “Frequency-driven market mechanisms for optimal dispatch in power networks.” [Online]. Available: http://carmenere.ucsd.edu/jorge/publications/data/2020_StChPeScCo-auto.pdf
- [13] C. D. Persis and N. Monshizadeh, “A feedback control algorithm to steer networks to a cournot–nash equilibrium,” *IEEE Transactions on Control of Network Systems*, vol. 6, no. 4, pp. 1486–1497, 2019.
- [14] L. Martini, H. Brunner, E. Rodriguez, C. Caerts, T. I. Strasser, and G. M. Burt, “Grid of the future and the need for a decentralised control architecture: the web-of-cells concept,” *CIREP - Open Access Proceedings Journal*, vol. 2017, no. 1, pp. 1162–1166, 2017.
- [15] N. Lehmann, J. Huber, and A. Kiesling, “Flexibility in the context of a cellular system model,” in *2019 16th International Conference on the European Energy Market (EEM)*. IEEE, 2019, pp. 1–6.
- [16] T. Jouini, C. Arghir, and F. Dörfler, “Grid-friendly matching of synchronous machines by tapping into the dc storage,” *IFAC-PapersOnLine*, vol. 49, no. 22, pp. 192–197, 2016.
- [17] P. Monshizadeh, C. D. Persis, T. Stegink, N. Monshizadeh, and A. van der Schaft, “Stability and frequency regulation of inverters with capacitive inertia,” in *CDC*. New York: IEEE, 2018, pp. 5696–5701.
- [18] L. Kölsch, K. Wieninger, S. Krebs, and S. Hohmann, “Distributed frequency and voltage control for ac microgrids based on primal-dual gradient dynamics,” in *2020 IFAC World Congress*, 2020.
- [19] J. Machowski, J. W. Bialek, and J. R. Bumby, *Power system dynamics: Stability and control*, 2nd ed. Chichester: Wiley, 2012.
- [20] S. P. Boyd and L. Vandenberghe, *Convex optimization*, 18th ed. Cambridge: Cambridge Univ. Press, 2015.
- [21] K. J. Arrow, L. Hurwicz, and H. Uzawa, *Studies in Linear and Non-Linear Programming*. Redwood City: Stanford University Press, 1958.
- [22] A. Antipin, “Minimization of convex functions on convex sets by means of differential equations,” *Differential Equations*, vol. 30, no. 9, pp. 1365–1375, 1994.
- [23] M. T. M. Emmerich and A. H. Deutz, “A tutorial on multiobjective optimization: fundamentals and evolutionary methods,” *Natural computing*, vol. 17, no. 3, pp. 585–609, 2018.
- [24] IEEE, “57 bus test system.” [Online]. Available: <https://icseg.iti.illinois.edu/ieee-57-bus-system/>